Design of Parallel Variable Stiffness Actuators

Chase W. Mathews and David J. Braun

Abstract—Direct-drive motors (DDMs) have been increasingly used for robot actuation because they provide high-fidelity torque control, but they typically have low torque density. Gearing can be used to increase the torque density of motors, but gearing decreases the power density of the actuator. Parallel elastic actuators (PEAs), composed of a spring attached in parallel to a motor, can increase both the torque and power density of the actuator without jeopardizing torque control fidelity. Parallel elastic actuators can also generate efficient oscillatory motion by applying the torque of the motor through resonant oscillations. However, conventional fixed stiffness springs used in PEAs only enable efficient oscillatory motion at a fixed resonant frequency defined by the stiffness of the spring. In this paper, we present a parallel variable stiffness actuator (PVSA) consisting of a directdrive motor connected in parallel to a variable stiffness spring. Parallel variable stiffness actuators retain the torque control bandwidth of DDMs and PEAs and can be used to amplify the torque and power of the motor over a range of oscillation frequencies. We present a compact design of a PVSA where a direct-drive motor, a high energy density composite spring, and a variable stiffness mechanism are arranged in a conventional cylindrical geometry, similar to a motor-gearbox assembly. We foresee the use of PVSAs in mobile robots and wearable devices, where energy efficient oscillatory motion at different frequencies, along with high torque and power density is indispensable.

I. INTRODUCTION

The endeavor to advance the performance and autonomy of robots has been limited by the lack of high-performance actuators [1]. One of the most commonly used actuators in robots are electric motors. State-of-the-art electric motors generate peak power when operated under nominal conditions: high speed and low torque. However, in most typical robot control tasks, such as pick and place tasks or locomotion tasks, the robot has to produce high torque at low speeds.

The traditional solution to address the aforementioned issue is to add a gearbox to the motor in order to reduce the speed and increase the torque. However, gearing also reduces the power density of the actuator, because gearing adds weight without increasing the power output of the actuator. Furthermore, the efficiency of an electric motor is task dependent; for example, electric motors are significantly less efficient in oscillatory tasks compared to non-oscillatory constant-speed

C. W. Mathews and D. J. Braun are with the Advanced Robotics and Control Laboratory within the Center for Rehabilitation Engineering and Assistive Technology, Department of Mechanical Engineering, Vanderbilt University, Nashville, TN 37235. E-mail: chase.w.mathews@vanderbilt.edu and david.braun@vanderbilt.edu. (Corresponding author: David J. Braun).

This work was supported in part by a Seeding Success Grant provide by Vanderbilt University and the National Science Foundation CAREER Award under Grant No. 2144551. The authors gratefully acknowledge the support.

This paper has supplementary downloadable multimedia material available at http://ieeexplore.ieee.org. The video demonstrates the working principle of the parallel variable stiffness actuator. The size of the video is 40 MB.

This paper was presented in part at the IEEE/RSJ International Conference on Intelligent Robots and Systems, Prague, Czech Republic, September 27 - October 1, 2021.

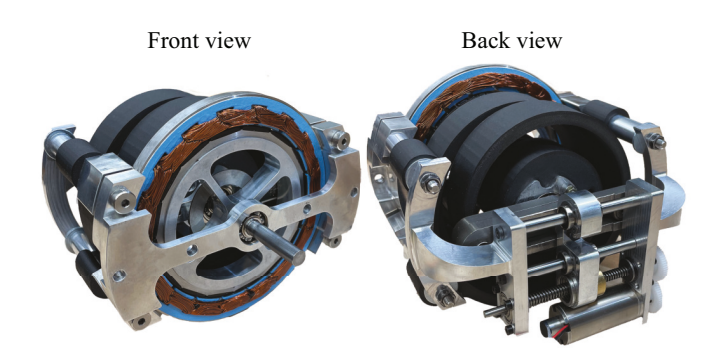


Fig. 1. Prototype parallel variable stiffness actuator (PVSA).

tasks. High torque density, power density, energy efficiency, and torque control fidelity are all important features for mobile and wearable robots. However, designing an actuator that displays the majority of these features has been a challenge.

Motors with low gear ratios have been used in applications where high gearing could compromise power density, for example, in bipedal walking [2], quadruped robot jumping and running [3], pick-and-place manipulation [4], and human assistive devices [5], [6]. However, the low torque density of direct-drive motors (DDMs) necessitates the use of a large motor to provide the torque required for pick-and-place, manipulation, and locomotion tasks. Unlike gearing, springs can provide both torque and power amplification to enhance the performance of motors. For example, in dynamic oscillatory tasks, such as the arm swinging to throw or the leg swinging to walk, run, and jump [7]–[15], springs can be used to amplify the torque and power of a relatively small motor.

One way to incorporate a spring into an actuator is to couple the spring between the motor and the load. This is a typical arrangement, reminiscent of series elastic actuators (SEAs) [16] and variable stiffness actuators, or more precisely, serial variable stiffness actuators (SVSAs) [17]–[19]. Series elastic actuators can be found in arm exoskeletons [20] and lower limb prostheses [21]–[23], while SVSAs can be found in ankle exoskeletons [24], [25] and robotic joints [9], [26]. Series elastic actuators and SVSAs are commonly used in the aforementioned applications due to their ability to track a desired motion similar to motors but with added compliance. However, since the force of the spring transfers through the motor in SEAs and SVSAs, these actuators require a large motor or an efficient, high-ratio gear reducer to generate large torques [27].

Another way to incorporate a spring into an actuator is to couple the spring to the load in parallel with the motor. Parallel elastic actuators (PEAs) have been widely used in static tasks. An example of a static task is gravity compensation, where the parallel spring can provide force at no energy cost to offload

the motor [28]. However, to provide gravity compensation at a desired position for different loads, PEAs require switchable springs or springs with changeable stiffness [29], [30].

In addition to static tasks, PEAs show significant promise in dynamic tasks. An example of a dynamic task is locomotion, where parallel springs have been used in assistive devices to passively offload force from human muscles; for example, the walking exoskeleton [10] and the jogging exoskeleton [11] utilized springs to reduce human metabolic energy cost. Parallel elastic actuators have been also used to reduce the energy needed to decelerate a load and to increase the peak power of a motor [31]-[37]. However, PEAs provide the most effective force and power amplification at the resonant frequency of the actuator and the load, or a narrow band of frequencies around the resonant frequency of the actuator and the load [38]. Therefore, to provide effective force and power amplification at variable desired oscillation frequencies, PEAs may tune the resonant frequency of the actuator and the load by means of switchable springs [39] or a variable stiffness mechanism.

In this paper, we introduce a parallel variable stiffness actuator (PVSA) which consists of a direct-drive motor arranged in parallel with a variable stiffness spring, shown in Fig. 1. The actuator has a compact design in which a DDM, a high-energy density composite spring, and a variable stiffness mechanism are arranged into a conventional cylindrical geometry, similar to a geared motor. The actuator retains the torque control bandwidth of DDMs, and can be used to maximize the output power over a range of oscillation frequencies. In Section II, we theoretically predict that PVSAs operated at resonance are faster and more energy efficient at accumulating energy than PEAs operated away from resonance, and are more effective at amplifying torque and power than both PEAs and DDMs. In Section IV, we experimentally validate our theoretical prediction by comparing a PVSA with a PEA and a DDM during an oscillatory task, where all three actuators are used to swing a robot-leg. We find that, because PVSAs can operate at a range of resonant frequencies, they provide a compliant alternative of controllable-speed geared motors, similar to PEAs providing a compliant alternative of constantspeed geared motors.

This paper extends our recent work [40], that introduced the concept of PVSAs, in three important ways: (i) first, we theoretically show the key benefit of PVSAs in oscillatory motion compared to PEAs and DDMs in Section II, (ii) second, we detail the prototype design and experimentally characterize the proposed PVSA in Section III, and (iii) finally, we experimentally verify the theoretically predicted benefits of our prototype PVSA compared to a PEA and a DDM in Section IV. We end the paper in Section V, where the results are discussed along with the limitations and further implications to create a compact and modular compliant actuator which can generate efficient oscillatory motion over a range of oscillation frequencies.

II. THEORETICAL PREDICTION

In this section, we (i) show the simplest mathematical model of parallel variable stiffness actuators (Section II-A), (ii) define a typical oscillatory task that could benefit from the use of PVSAs (Section II-B), (iii) list the practical limitations of PVSAs (Section II-C), (iv) discuss the benefit of using parallel springs over series springs for oscillatory tasks (Section II-D), (v) establish the benefit of adaptable stiffness over fixed stiffness spring actuation (Section II-E), and (vi) analyze the energy cost of stiffness adaptation in PVSAs (Section II-F).

A. Mathematical model

The model of a parallel variable stiffness actuator is shown in Fig. 2. The model consists of a direct-drive motor (red), load (blue), variable stiffness spring and the motor used to modulate the spring stiffness (green).

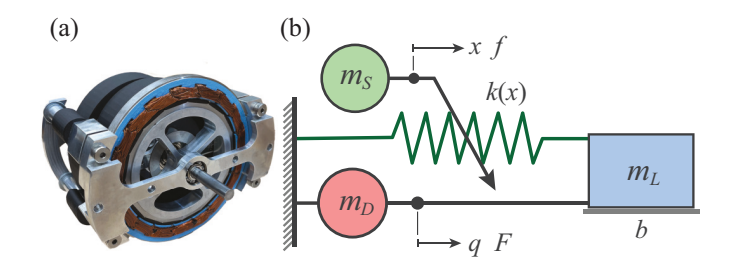


Fig. 2. (a) Parallel variable stiffness actuator. (b) Model of the actuator.

The simplest mathematical model of the PVSA is represented with the governing equations that describe the dynamics of the load and the dynamics of the mechanism used to change the spring stiffness,

$$(m_L + m_D)\ddot{q} + b\dot{q} + k(x)q = F, \tag{1}$$

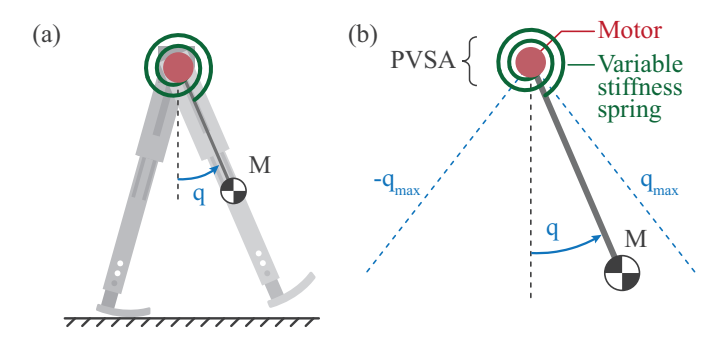
$$m_S \ddot{x} = F_S - \frac{1}{2} \frac{dk(x)}{dx} q^2,$$
 (2)

where m_L is the mass of the load, m_D is the mass of the directdrive motor, q is the position of the motor and the load, b is the damping of the motor and the load, k is the spring stiffness, F is the force provided by the direct-drive motor to move the load, m_S is the mass of the mechanism that modulates the spring stiffness, x is the position of the stiffness modulating motor, while F_S is the motor force used to modulate the spring stiffness. The relation between the spring stiffness and the motor position k = k(x) can be linear or non-linear depending on the design of the actuator [41].

In the remainder of this section, we present a simple theoretical analysis using the following two assumptions: (A1) The relation between the motor position and the stiffness of the spring is linear: $k(x) \propto x$. Based on (A1), we use the stiffness as the control variable in (1). (A2) The spring stiffness is only modulated when the spring does not store energy, and as such, when the spring does not impart force on the stiffness modulating motor: $q \approx 0$. Based on (A2) and (1), we consider the energy cost of changing stiffness negligible compared to the energy stored by the spring [41], [42]. We will substantiate the theoretical predictions made using assumptions (A1) and (A2) with experimental data presented in Section IV.

B. Using PVSAs for oscillatory tasks

Consider a typical oscillatory task, for example, a locomotion task such as walking, where the leg swings forward and backward, see Fig. 3. In this task, performance, such as speed, is directly related to the swing frequency. Consequently, an actuator that can increase swing frequency using a torque limited direct-drive motor while keeping the maximal joint angle the same could potentially improve performance (such as increasing walking speed). A similar argument may be extended to a pick and place task or other oscillatory tasks.



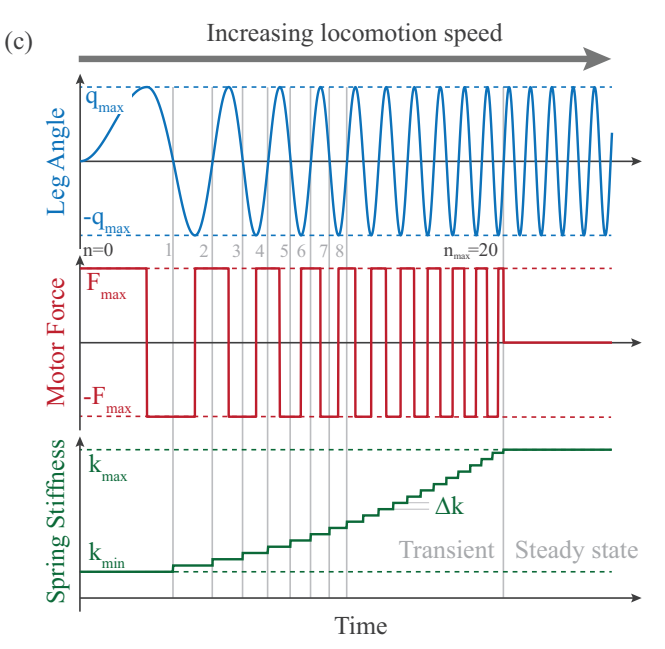


Fig. 3. (a) Model of walking. (b) Model of the hip, augmented by a PVSA. (c) Leg-angle, motor force, and spring stiffness versus time as the oscillation frequency increases.

In order to demonstrate to use of a PVSA, we aim to increase the frequency of oscillations (Fig. 3c) using a limited force provided by the direct-drive motor F while keeping the motion of the load q limited:

$$F \in [-F_m, F_m]$$
 and $q \in [-q_{\text{max}}, q_{\text{max}}].$ (3)

Increasing the oscillation frequency, while the amplitude of the oscillator is limited, can be achieved by increasing the mechanical energy of the load.

The theory of linear (and non-linear) oscillators suggests that we can maximize the amount of energy provided by the direct-drive motor to the load by using the following switching control law:

$$F \in \left\{ \begin{array}{ll} +F_m & \text{if} \quad \dot{q} \le 0 \\ -F_m & \text{if} \quad \dot{q} > 0 \end{array} \right., \tag{4}$$

where the motor force is limited, and the switching between the positive and negative force is performed when the oscillatory motion changes direction, see Fig. 3c (red). However, (4) alone would not keep the amplitude of the oscillatory motion limited to $q \in [-q_{\text{max}}, q_{\text{max}}]$.

In order to keep the amplitude of the oscillatory motion limited, we change the stiffness of the spring from k_n to k_{n+1} at each half oscillation cycle $n \in \mathbb{N}$, see Fig. 3c (green). The change in stiffness is defined by the work-energy principle. For a linear un-damped oscillator, we obtain:

$$\frac{1}{2}(k_{n+1} - k_n)q_{\max}^2 = 2F_m q_{\max},\tag{5}$$

where we assume that the stiffness changes instantaneously when the spring does not store energy q = 0 (assumption (A2) in Section II-A). According to (5), we find the following stiffness adaptation law:

$$k_{n+1} = k_n + \Delta k$$
 and $\Delta k = \frac{4F_m}{q_{\text{max}}},$ (6)

where the increment in the spring stiffness Δk depends on the force applied by the direct-drive motor F_m , and the maximal amplitude of the oscillations q_{max} , see Fig. 3c (green).

Using the force control law (4) and stiffness adaptation law (6), we obtain the following results:

(i) For any $\Delta k \ge 4F_m/q_{\rm max}$, the motion of the un-damped linear oscillator will remain feasible, while for $\Delta k = 4F_m/q_{\rm max}$, the amplitude will be maximized in every oscillation cycle, as shown in Fig. 3c (blue):

$$\forall t \in (0, \infty) : \dot{q}(t) = 0, \ |q(t)| = q_{\text{max}};$$

(ii) The stiffness of the spring increases according to the following relation, see Fig. 3c (green):

$$k_n = \frac{2F_m}{q_{\text{max}}}(1+2n);$$
 (7)

(iii) The combined force of the spring and the motor is amplified according to the following relation:

$$|F_n| = |F_m| + k_n q_{\text{max}} \Rightarrow \left| \frac{F_n}{F_m} \right| = 3 + 4n;$$
 (8)

(iv) The elastic potential energy stored by the spring accumulates proportional to the work done by the motor at each oscillation cycle $E_m = 2F_m q_{\text{max}}$:

$$E_n = 2F_m q_{\text{max}} n \Rightarrow \frac{E_n}{E_m} = n; \tag{9}$$

(v) The frequency of the load is increased according to:

$$\frac{f_n}{f_m} = \frac{\frac{1}{2\pi} \sqrt{\frac{k_n}{m_L + m_D}}}{\sqrt{\frac{F_m}{32(m_L + m_D)q_{\text{max}}}}} = \frac{4}{\pi} \sqrt{1 + 2n};$$
 (10)

where f_m is the frequency of a square-wave force required to generate oscillatory motion with amplitude q_{max} in absence of the spring.

(vi) The average mechanical power of the spring per oscillation cycle is amplified according to the following relation:

$$\frac{p_n}{p_m} = \frac{E_n f_n}{E_m f_m} = \frac{4n}{\pi} \sqrt{1 + 2n}.$$
 (11)

In (8)–(11), F_m is the maximal force, E_m is the maximal energy, f_m is the maximal frequency, and p_m is the maximal power if the direct-drive motor is used alone to oscillate the load under the amplitude limitation given in (3). Consequently, (8)–(11) can be used to compare the parallel variable stiffness actuator and the direct-drive actuator in the considered task.

The theoretical results predict that a parallel variable stiffness spring can amplify force similar to a (3+4n): 1 gearbox (8), but unlike a gearbox, it can also accumulate energy (9), increase the frequency (10), and amplify the power of the motor (11). However, (8)–(11) do not show the limitations of a PVSA in increasing force, energy, frequency, and power, as the number of oscillations increases, shown in Fig. 3(c). We discuss these limitations in the next section.

C. What limits a parallel variable stiffness actuator?

In this subsection, we list three main practical limitations of a parallel variable stiffness actuator:

(L1): In Section II-B, we neglected the time required to change the motor force in (4), the time delay in detecting the sign change of the velocity in (4), and the time required to change the spring stiffness k in (6).

We can neglect these effects by assuming that each half-cycle of the oscillatory motion (Fig. 3c) takes at least an order of magnitude longer than the time-constant of the direct-drive motor τ_q (Fig. 2b red), the time-delay in detecting zero velocity δt in (4), and the time-constant of the closed-loop position dynamics of the stiffness adjusting motor τ_x (Fig. 2b green):

$$\tau_a f_n \ll 1, \quad \delta t f_n \ll 1, \quad \tau_x f_n \ll 1.$$
 (12)

(L2): The ability of a PVSA to accumulate energy is restricted by the limited amplitude of the oscillatory motion $q \in [-q_{\max}, q_{\max}]$ and the finite stiffness of the spring:

$$k_n = \frac{2F_m}{q_{\text{max}}}(1+2n) \in [k_{\text{min}}, k_{\text{max}}].$$
 (13)

Using (13) and (6), we find the upper bound on the number of oscillation cycles that can be used to accumulate energy n_{max} within the limited amplitude of the oscillator (see Fig. 3c):

$$0 \le n \le n_{\text{max}} = \frac{1}{2} \left(\frac{k_{\text{max}}}{k_{\text{min}}} - 1 \right).$$
 (14)

(L3): The ability of a PVSA to accumulate energy is also limited by energy dissipation; the work done by the motor in each half-cycle of the oscillatory motion must be greater than the energy dissipated during the same half-cycle of the oscillatory motion:

$$2F_m q_{\text{max}} \ge b \int_0^{\frac{1}{2f_n}} \dot{q}_n(t)^2 dt.$$
 (15)

We estimate the integral in (15) assuming a small energy loss compared to the energy stored by the spring; we assume a small damping ratio $\zeta = b/4\pi f_n(m_L + m_D) \ll 1$,

and use the velocity of the un-damped oscillator $\dot{q}_n(t) = 2\pi f_n q_{\rm max} \cos(2\pi f_n t)$ and the frequency of the un-damped oscillator $f_n = \frac{1}{2\pi} \sqrt{k_n/(m_L + m_D)}$ (10), where k_n is defined in (7). As a result, we obtain an upper bound of the minimal force for the direct-drive motor:

$$F_m \ge \frac{\pi^2}{8} \frac{b^2 q_{\text{max}}}{m_I + m_D} (1 + 2n).$$
 (16)

Using (16) and (8), we find that the presence of damping limits the maximal number of oscillation cycles n_{max} during which energy can be accumulated:

$$0 \le n \le n_{\text{max}} \approx \frac{1}{2} \left(\frac{8F_m(m_L + m_D)}{\pi^2 b^2 q_{\text{max}}} - 1 \right). \tag{17}$$

In summary, (14) and (17) reveal that the maximal force amplification of a variable stiffness spring is limited by the maximal stiffness range and the internal damping of the actuator. Therefore, increasing the stiffness range and reducing the internal damping are two important ways to increase the force, energy, frequency, and power amplification capability of a parallel variable stiffness actuator.

D. What is the benefit of parallel versus series springs?

To explore the difference between parallel and series spring actuators in the context of a resonant oscillatory task, we examined the ability of these actuators to emulate a spring.

For an ideal spring-mass system, the maximal energy transferred to the load E_L and the maximal energy stored by the spring E_S are equal during constant-amplitude and constant-frequency oscillations; $E_L/E_S=1$ (steady-state portion of Fig. 3c). In Section VI-A, we derived the same energy ratio, denoted by $E_L/E_S|_P$ and $E_L/E_S|_S$ for optimally tuned direct-drive PVSAs (or optimally designed PEAs) and optimally tuned geared SVSAs (or optimally designed SEAs) that use an $n_G:1$ gear reducer between the motor and the spring (optimally designed and tuned means that the spring stiffness is chosen such that the actuator is operated at resonance):

$$\frac{E_L}{E_S}\Big|_P = \frac{1}{1 + \frac{m_D}{m_L}} \quad \text{and} \quad \frac{E_L}{E_S}\Big|_S = \frac{n_G^2 \frac{m_D}{m_L}}{1 + n_G^2 \frac{m_D}{m_L}}.$$
 (18)

According to (18), a direct-drive parallel spring actuator can behave similar to an ideal spring, as it can transfer almost all the energy stored by the spring to the load, assuming the motor mass is much smaller than the load mass $(m_D \ll m_L)$. The same applies to series spring actuators if the gear reduction ratio between the motor and the spring is high enough $(n_G \ge m_L/m_D)$. While (18) shows that series spring actuators can reach even higher energy transfer ratios than parallel spring actuators $(\lim_{n_G \to \infty} E_L/E_S|_S = 1)$, (18) also shows that series spring actuators must use a large gearbox $(n_G \ge m_L/m_D)$ to efficiently transfer the energy stored by the spring to the load. A large gearbox introduces added mass, lower power density, longer transient time to accumulate energy (transient portion of Fig. 3c), and may also increase energy dissipation.

We note that, in some cases, the increased energy dissipation due to gearing can be minimized in series spring actuators by holding the motor stationary [43], [44] – assuming that the small motor force $F \in [-F_m, +F_m]$ acting through a large $n_G : 1$ gearbox can counteract the spring force $n_G F_m \ge k_n q_{\max}$. Such scenario only applies to a spring-mass system that oscillates at constant-amplitude and constant-frequency with no load-side damping, as in that case, the motor is not required to do work. During transient energy accumulation (transient portion in Fig. 3c) or in the presence of load-side damping (b > 0 in (16)), the motor must move to do work, and as such it is subject to increased energy dissipation due to gearing.

E. What is the benefit of stiffness adaptation?

If the motor is used to oscillate the load with the desired amplitude at a non-resonant frequency, then the energy supplied by the motor will be more than the energy supplied by the motor at resonance. In order to quantify the energetic benefit of resonant versus non-resonant oscillations, we estimate the maximal mechanical efficiency of parallel spring actuators η_{Pm} by using the maximal kinetic energy of the load divided by the maximal elastic potential energy stored by the spring and the minimal energy that must be supplied by the motor:

$$\eta_{Pm} = \frac{E_L}{E_S + E_D} \approx \frac{\frac{1}{2} m_L \dot{q}_{\text{max}}^2}{\frac{1}{2} k q_{\text{max}}^2 + \int_0^{\frac{1}{2f}} |F \dot{q}| dt}.$$
 (19)

To compute the minimal amount of energy supplied by the motor, E_D , we neglect Joule losses and assume that the direct-drive motor does not regenerate negative work; the motor supplies energy to both accelerate and decelerate the load. As such, the energy supplied by the motor is estimated using the absolute value of the mechanical power.

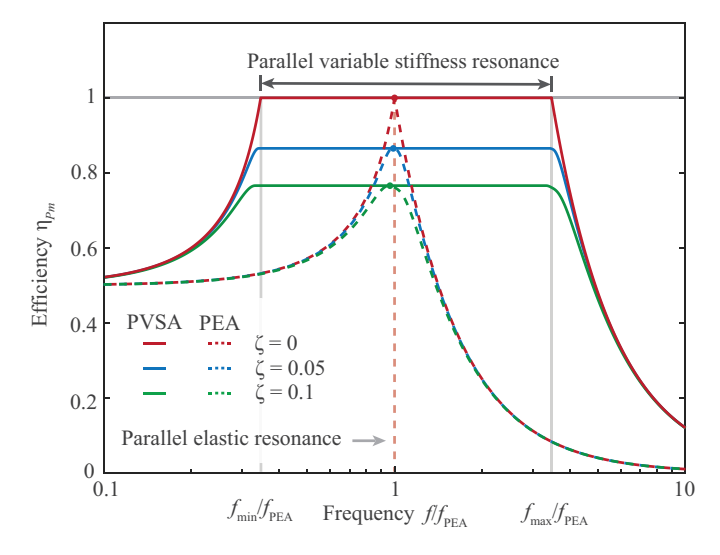


Fig. 4. Mechanical efficiency of parallel elastic actuators (dashed lines) and parallel variable stiffness actuators (solid lines) at different damping ratios ζ .

Figure 4 shows the efficiency (19) of a PVSA (solid lines) and a PEA (dashed lines) as a function of the oscillation frequency f/f_{PEA} , where $f_{\text{PEA}} = \frac{1}{2\pi} \sqrt{k_{\text{PEA}}/(m_L + m_D)}$, and the damping ratio is small, $\zeta \ll 1$. According to Fig. 4, the PVSA is able to maintain peak efficiency for a large range of frequencies $f \in [f_{\min}, f_{\max}]$, determined by the stiffness range of the variable stiffness spring $k \in [k_{\min}, k_{\max}]$, while the

PEA can only reach peak efficiency at one frequency f_{PEA} , determined by the fixed stiffness of the spring k_{PEA} . However, tuning the stiffness of a PVSA to different resonant frequencies costs energy. We will next show that the energy cost of tuning the stiffness of PVSAs is negligible compared to the energy supplied by the direct-drive motor and stored by the spring.

F. What is the energy cost of stiffness adaptation?

Up to now, we have assumed that the stiffness of the spring is changed when the spring stores no energy q=0, such that the energy cost of changing the spring stiffness can be kept negligible compared to the energy supplied by the direct-drive motor – because in this case, the stiffness adjusting motor does not need to do work against the spring. In practice, changing the spring stiffness cannot be done instantaneously, and therefore, it can only be done when the spring stores some energy $q\approx 0$. Consequently, it is of interest to investigate whether the energy cost of changing the spring stiffness each half-cycle of the oscillatory motion can be kept negligible compared to the energy supplied by the direct-drive motor during the same half-cycle of the oscillatory motion.

In order to estimate the energy cost of changing the spring stiffness during one oscillation cycle, we compute the maximal amount of energy to increase the spring stiffness by $\Delta k \geq 0$, as the spring deforms from q=0 to $q=\Delta q \ll q_{\rm max}$,

$$\Delta E_k \le \frac{1}{2} \Delta k \Delta q^2.$$

Subsequently, we define the ratio between ΔE_k and the energy supplied by the direct-drive motor $\Delta E_n = 2F_m q_{\text{max}} = \frac{1}{2}\Delta k q_{\text{max}}^2$ (5) during the same half-cycle of the oscillatory motion:

$$\frac{\Delta E_k}{\Delta E_n} \le \left(\frac{\Delta q}{q_{\text{max}}}\right)^2 \ll 1. \tag{20}$$

Inequality (20) suggests that the energy cost of increasing the spring stiffness while the spring is deflected by $\Delta q \ll q_{\rm max}$ is negligible compared to the energy supplied by the direct-drive motor. In Section VI-B, we estimated the energy to accelerate (and decelerate) the stiffness adjusting motor, as required to change the spring stiffness. We found that with a properly designed stiffness modulating mechanism, the energy cost of accelerating (or decelerating) the motor can be negligible compared to the energy supplied by the direct-drive motor. Our experiment corroborates these theoretical predictions (see Section IV, Fig. 12).

III. DESIGN OF THE PROTOTYPE

In this section, we present a prototype parallel variable stiffness actuator. The design of the actuator is shown in Fig. 5. The actuator fits into a cylindrical geometry similar to a motor-gearbox assembly. The actuator consists of three main components: the direct-drive motor, the custom-built composite spring, and the variable stiffness mechanism. The main specifications of the prototype are given in Table I.

In the following, we detail the design of each component.

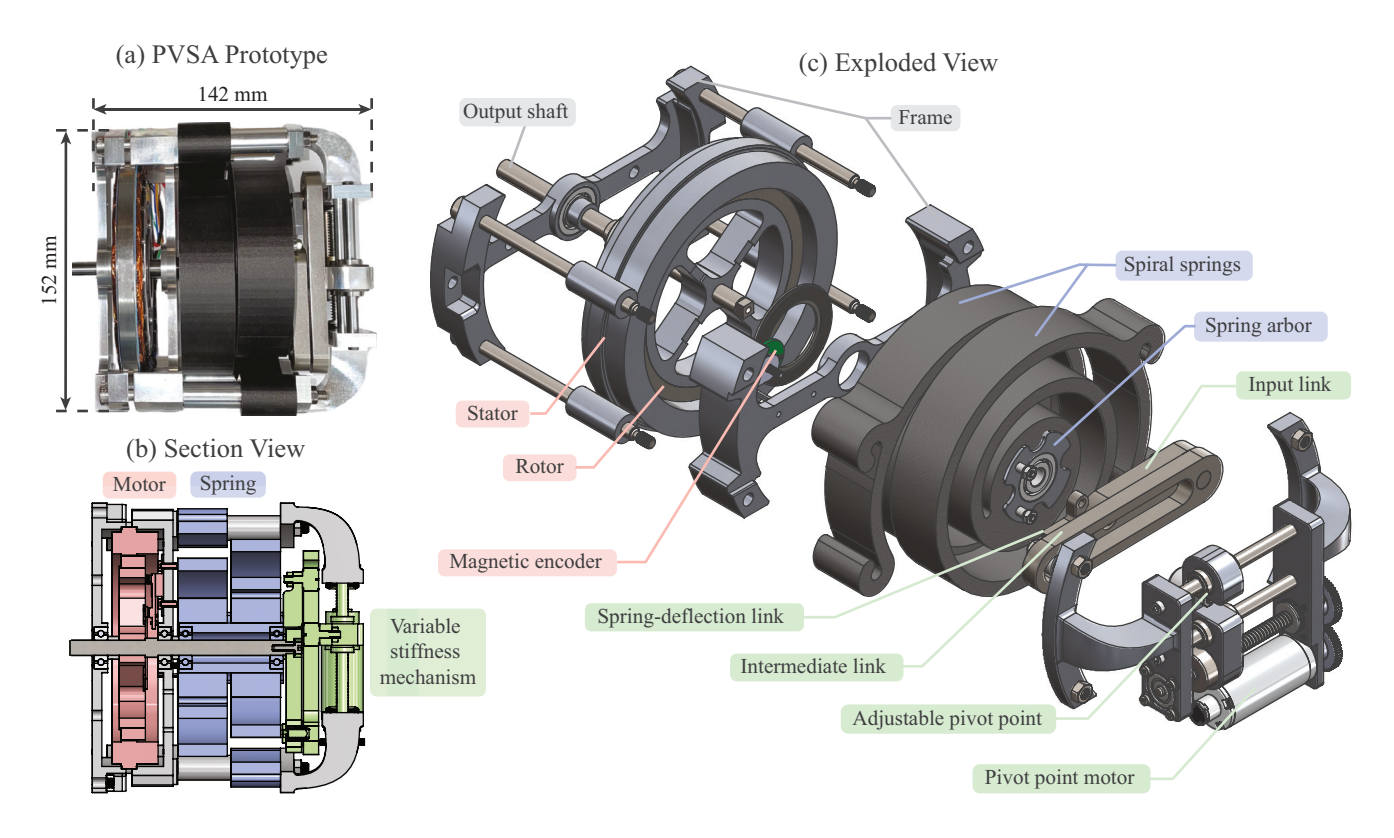


Fig. 5. Design of the prototype parallel variable stiffness actuator. (a) Top view. (b) Section view. (c) Exploded view.

ACTUATOR PARAMETERS		
Name	Value	Unit
Diameter	152	(mm)
Width	142	(mm)
Total mass	1.9	(kg)
Maximum deflection	\pm 45	(deg)
Stiffness range	[1.9, 29.3]	$(Nm \ rad^{-1})$
Average rate of stiffness change	28.7	$(Nm \ rad^{-1}s^{-1})$
Maximum torque of the drive motor	1.6	(Nm)
Maximum torque of the actuator	18	(Nm)

TABLE I

A. Direct-drive motor

The actuator is driven by an Allied Motion MF0127008 brushless frameless motor shown in Fig. 6. The motor weighs 0.5 kg and provides 1.6 Nm of continuous torque. The motor is supported by the aluminum housing shown in Fig. 5c. The rotation angle of the motor shaft is measured by an AMS AS5304A offset-axis magnetic encoder and a 64-pole RLS MR045 axial magnetic ring shown in Fig. 5c. The direct-drive motor was driven using an Allied Motion SXD drive.

In a PVSA, the maximal motor torque defines the number of oscillation cycles to reach the desired oscillation frequency. However, to reach the desired frequency, the motor must also generate enough torque to overcome the energy loss while moving the load (17). In PVSAs, the motor torque does not define the maximum output torque and the motor power does not limit the maximum output power of the actuator; both can be amplified if the spring has a large enough energy storage capacity (13).

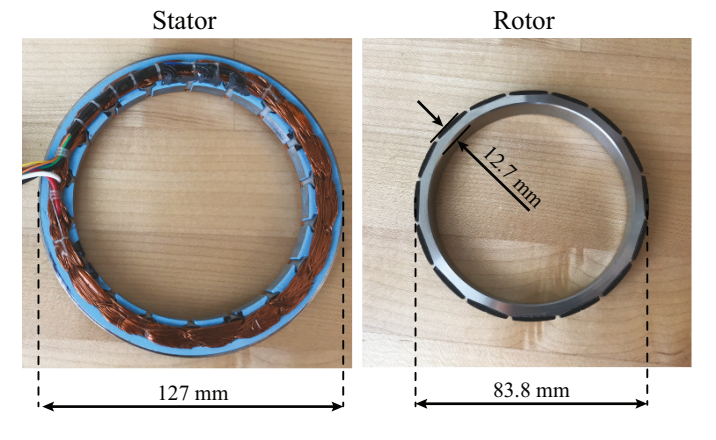


Fig. 6. Direct-drive motor.

B. Torsional spring

The actuator embodies two torsional composite springs shown in Fig. 7. The springs are connected to the shaft through the stiffness modulating mechanism and are fixed at the aluminum housing shown in Fig. 5.

The springs were 3D printed via a Markforged Mark Two printer. The print was reinforced with 20% continuous strands of fiberglass (Fig. 7b). The springs weigh 227 g each, can be deflected by 95 deg, and provide a maximum of 3 Nm of torque. The combined energy storage capacity of the springs is 5 J.

With continuous fiber reinforced 3D-printing, strands of fiberglass, carbon fiber, or Kevlar can be laid along the length

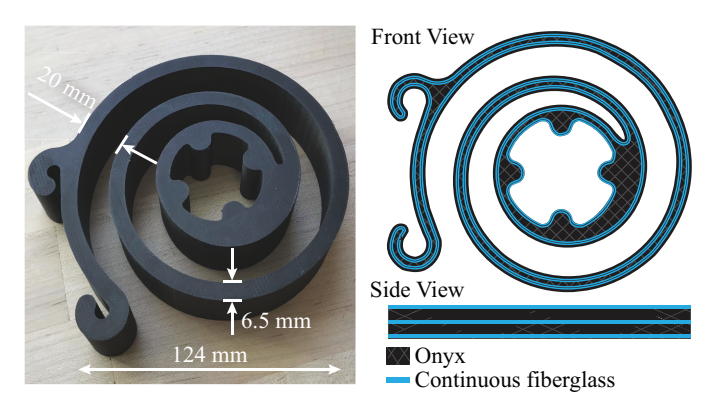


Fig. 7. 3D printed torsion spiral spring. The right figure shows the continuous fiberglass layout of the 3D printed spring. The top-down view shows the two concentric fibers. The side view shows the distribution of layers reinforced with fiberglass (blue) and the layers made of Onyx (a mixture of plastic and chopped carbon fiber) material.

of the spiral spring [45]. The fiberglass material used to create the torsional spring has an elastic strain energy density of 685 J/kg in flexion as compared to 86 J/kg for AISI 1095 spring steel. We leveraged this 3D printing technology to create high-energy density springs with customizable mechanical properties adjusted by increasing the fiber infill, thickness, and length [46].

We use a spiral form factor because of the ease of 3D printing as well as a relatively large volumetric energy density. The relation between the torsional stiffness of a spiral spring and the geometric and material properties of the spring are given by [47]:

$$k_{\text{spring}} = \frac{Ebh^3}{12L},\tag{21}$$

where E is Young's modulus of the spring material, b is the spring width, h is the spring thickness, while L is the length of the spring. The torsional stiffness of the two printed spiral springs was estimated to be 5.85 Nm/rad.

Flat spiral springs do not necessarily have the same properties in counterclockwise rotation as in clockwise rotation. One way to account for the asymmetry in the torque-deflection curve is by de-clutching one of the two springs experiencing extension [48]. However, this results in reduced energy density, since one spring is disengaged at all times. Another way to account for the asymmetry in the torque-deflection curve is to mount two springs in opposite configurations such that one is in extension while the other is in compression. In this setup, the torque-deflection curve will be symmetric in compression and extension. Such arrangement is used in our device.

C. Variable stiffness mechanism

The prototype PVSA embodies a variable stiffness mechanism shown in Fig. 8a. The mechanism embodies a lead screw, with length of 84 mm and lead of 1.6 mm, driven by a 10 W Maxon DCX22L motor. The motor is controlled using a Maxon ESCON 50/5 drive.

The variable stiffness mechanism consists of three linkages: the shaft link (orange), the intermediate link (green), and the spring deflection link (blue), shown in Fig. 8b. The shaft link (orange) is rigidly connected to the main shaft and rotates the intermediate link (green) about the pivot point (the position of the pivot point is denoted by x). The pivot point is moved by the lead screw (gray). As a result, the intermediate link (green) rotates the spring deflection link (blue) to create an angular deflection on the spring (light blue). By regulating the position of the pivot point x via a linear actuator, the mechanical advantage of the spring is adjusted, and therefore, the stiffness of the spring seen from the shaft link (orange) is controlled.

The mechanism is a rotary version of the variable pivot-point lever arm mechanism used in the AWAS-II actuator [49]. To convert the variable pivot point lever arm from a linear spring to a torsional spring setup, two linkages are added to relate the shaft angle θ to the spring deflection angle α , as depicted in Fig. 8b. The geometric relationship between the shaft angle θ and the spring angle α is defined by computing the tangent of the intermediate link angle β (Fig. 8b) for each side of the pivot point:

$$f_{\rm in}(\theta) = \frac{d\sin\theta}{l - x + d\cos\theta} = \tan\beta = \frac{l\sin\alpha}{x - l + l\cos\alpha} = f_{\rm out}(\alpha),$$
(22)

where d is the length of the shaft link, l is the length of the spring link, while x is the position of the pivot point. Using (22) as an implicit relation between the shaft angle and the spring angle $\alpha = \alpha(\theta, x)$, we define the shaft torque:

$$\tau = \left(\frac{\frac{df_{\text{in}}(\theta)}{d\theta}}{\frac{df_{\text{out}}(\alpha)}{d\alpha}}\right) k_{\text{spring}} \alpha(\theta, x), \tag{23}$$

where k_{spring} is the torsional stiffness defined by (21) and $x \in [0, x_{\text{max}}] = [0, l+d]$ is the position of the pivot point. The torque-deflection curves corresponding to different pivot point positions, different $x \in [0, x_{\text{max}}]$, are shown in Fig. 8c.

The stiffness of the mechanism is defined by the slope of the torque deflection curves at the origin in Fig. 8c, and can be obtained by linearizing (23):

$$k(x) = \frac{\partial \tau}{\partial \theta} \bigg|_{\theta=0} \approx k_{\text{spring}} \left(\frac{x}{l+d-x}\right)^2.$$
 (24)

The theoretical stiffness range of the mechanism is $k \in [0, \infty]$ where x = 0 provides zero stiffness while x = l + d leads to infinite stiffness. The usable range of the pivot point position is $x/x_{\text{max}} = [0.25, 0.75]$, and consequently, the practical stiffness range of the mechanism is $k/k_{\text{spring}} \in [0.1, 9]$.

We use a motor and lead screw assembly to quickly move the pivot point when the spring is near equilibrium $\theta \approx 0$ and does not impose a large force to the motor. In this case, the friction force of the lead screw is minimal, and the stiffness can be adjusted rapidly as if the spring would be disconnected from the actuator [41].

When deflected, the spring imposes a significant force on the lead screw used to change the pivot point position. However, because of the self-locking behavior of the lead screw [50], the motor does not experience any of the spring force, and does not require energy to hold a given pivot point position.

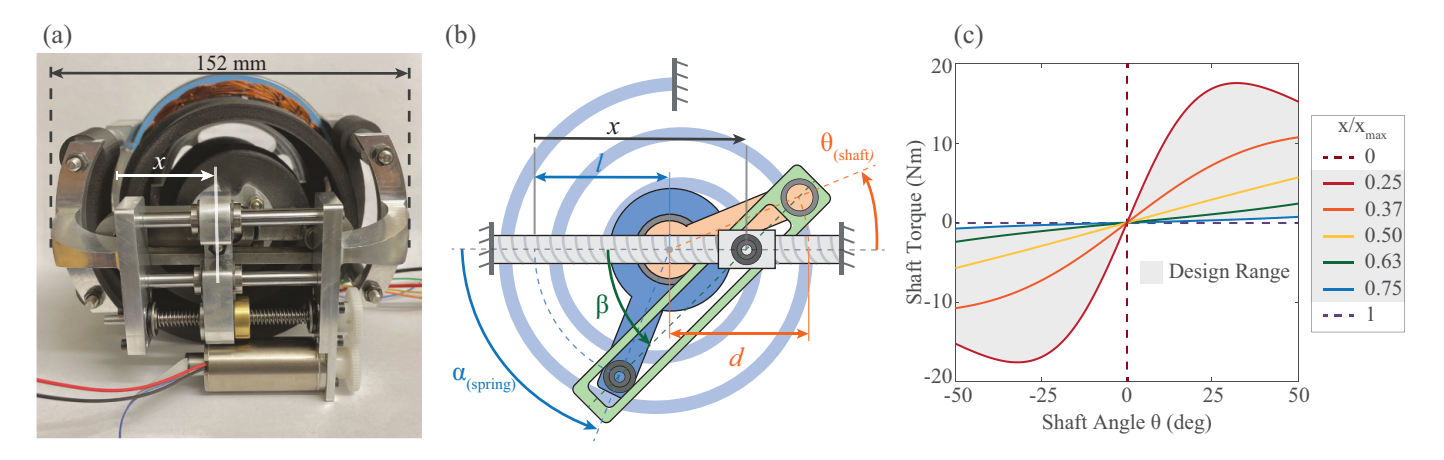


Fig. 8. (a) Prototype parallel variable stiffness actuator showing the motor-driven lead screw assembly. The position of the pivot point is labeled with x. (b) Variable stiffness linkage mechanism. The shaft link is orange. The spring link is blue. (c) Torque versus input deflection (shaft) angle θ for different pivot point positions. The feasible torque range achievable by the mechanism is shown with solid lines (the theoretical limits are shown with dashed lines).

D. Characterization

In order to validate the predicted torque deflection characteristic of the PVSA (Fig. 8c), we experimentally measured the torque of the actuator. In the experiment, the shaft of the actuator was deflected at least ± 30 deg at five different pivot-point positions $x \in [20, 30.25, 40.5, 50.75, 61]$ mm. The restoring torque was meanwhile measured using a load cell (Transducer Techniques MLP-50). The measurements were done quasi-statically; the spring was slowly deflected up to ± 30 deg for each pivot point setting.

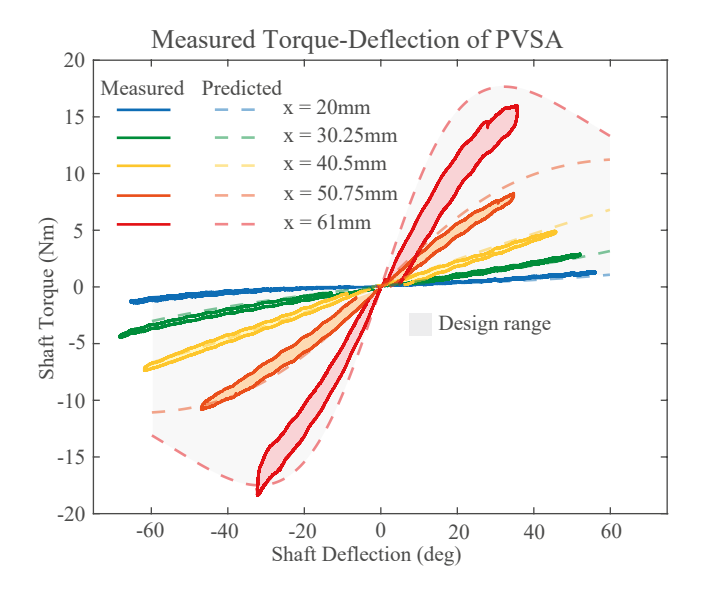


Fig. 9. Torque-deflection curves of the PVSA across five different stiffness values. The measured torques are shown with solid lines while the theoretically predicted torques are shown with dashed lines. The shaded loops show the energy loss during an extension-compression work cycle.

Figure 9 summarizes the experimental data: the solid lines show the measured torques while the dashed lines show the theoretically predicted torques. We observe a reasonable match between the measured and the theoretically predicted curves. The measured torques match the theoretically predicted torques to an average difference of 15% while the estimated

stiffnesses match the theoretically predicted stiffnesses to an average difference of 22%. We notice that the measured torque values are generally lower than the predicted torque values. The difference becomes more prominent under higher loads, and can be largely attributed to the finite structural rigidity of the actuator. Namely, the pivot point tends to move towards the lower stiffness configurations as the frame deforms under load, which leads to decreased stiffness.

In Fig. 9 we observe a hysteresis-loop between the torqueangle data in each loading cycle. The area inside the loop formed by the torque deflection curves represents the amount of energy dissipated by the actuator per loading cycle. In order to quantify the energy dissipation, we divided the amount of energy dissipated per loading cycle with the total energy stored by the spring per loading cycle. As a result, we calculated a 20% energy loss largely independent of the stiffness setting of the actuator. We found that the main source of energy dissipation is the composite spring and not the variable stiffness mechanism. This was confirmed by a free swing experiment where the spring was decoupled from the actuator, and no significant energy dissipation was observed.

IV. EXPERIMENTAL VALIDATION

In this section, we evaluate the performance of the prototype PVSA. We introduce the experimental setup, present the controller used to perform the experiment, and summarize the results.

A. Setup

Figure 10 shows the experimental setup: the robot leg and the PVSA. The leg is part of a human-driven robot introduced in [51]. The leg was coupled to the PVSA with a friction clamp. The PVSA was used as a hip spring in this setup to oscillate the robot leg. To characterize the performance of the actuator during the experiments, we measured the angle of the leg θ and the position of the pivot point x that defines the stiffness. We have also estimated the torque and power of the direct-drive motor and the power of the motor used to adjust the stiffness of the actuator. Finally, we computed

the net actuator torque τ_{PVSA} by separating the gravitational torque contribution of the load:

$$\tau_{\text{PVSA}}(t) = J_{leg}\ddot{\theta}(t) + m_{leg}gl_{cm}\sin\theta(t),$$

where J_{leg} is the moment of inertia of the leg, m_{leg} is the mass of the leg, l_{cm} is the distance from the shaft to the center of mass of the leg, while $\ddot{\theta}(t)$ is the acceleration computed from the measured leg angle $\theta(t)$.

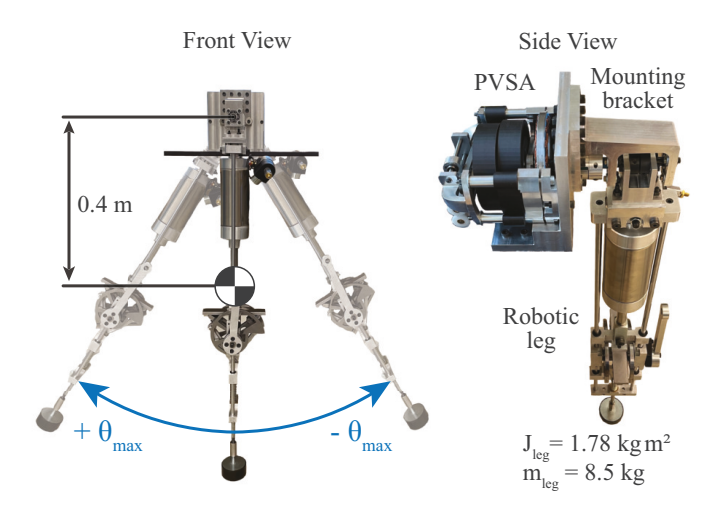


Fig. 10. Experimental setup. Front view: Robot leg. Side view: Parallel variable stiffness actuator. The leg has a total length of 0.95 m and a mass of 8.5 kg. The moment of inertia of the leg about the hip is 1.78 kg m².

B. Controller

In order to demonstrate the constant amplitude resonant actuation discussed in Section II-B, two controllers were developed. One of the controllers implemented resonant forcing (4) using the direct-drive motor (Fig. 6). The other controller implemented the stiffness adaptation law (6) using the small motor that changes the pivot point of the stiffness modulating mechanism (Fig. 8). The block-diagram of these controllers is shown in Fig. 11.

The controller used to adapt stiffness is represented by the green blocks in Fig. 11. The reference input to this controller is the desired stiffness. The desired stiffness k_d was converted into the desired pivot point position x_d using (24). The position of the pivot point x was regulated with a PD controller when the direct-drive motor was close to zero deflection $\theta \in [-5,5]$ deg.

The controller used to move the direct-drive motor is represented by the orange blocks in Fig. 11. The reference input to this controller is the desired maximal shaft angle $\theta_{\max}d$. The controller first estimated the maximal shaft angle θ_{\max} and then calculated the error between the estimated and desired maximal shaft angle. Based on the error, the controller either increased or reduced the constant motor torque used in each motion cycle τ_0 . The motor torque is subsequently compensated by taking into account the change in the stiffness of the actuator; increasing stiffness necessitates more torque $(\Delta \tau_0 > 0)$ while decreasing stiffness necessitates less torque $(\Delta \tau_0 < 0)$ to achieve the same oscillation amplitude. The

Stiffness control

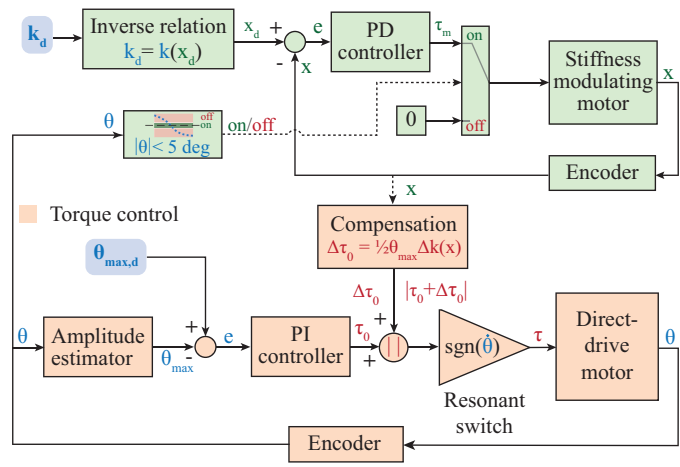


Fig. 11. Block-diagram of the controller. The controller was implemented in a custom dsPIC33F breakout board using Simulink Real-Time with a sampling frequency of 1 kHz.

compensation term $\Delta \tau_0$ was calculated assuming a linear torque deflection relation at the output shaft. The total torque $\tau = (\tau_0 + \Delta \tau_0) \text{sgn}(\dot{\theta})$ was used to implement the resonant control (4) of the direct-drive motor.

C. Results

In the experiments, the PVSA was used as a hip spring to oscillate the robot leg. In the first experiment, the robot leg was moved with constant amplitude but increasing frequency (as would be required in walking to increase speed while maintaining constant step length). In the second experiment, the robot leg was moved with constant frequency but increasing amplitude (as would be required in walking to increase speed while maintaining a constant stepping frequency). The actuator was able to store the same amount of energy in both experiments.

The experimental data is shown in Fig. 12. The left column of Fig. 12 shows the experiment performed with the PVSA while the right column shows the experiment performed with the PEA. The top row of the figure shows snapshots of the robot leg; the second row shows snapshots of the stiffness adjusting mechanism.

Figures 12(a-i), 12(a-ii), and 12(a-iii) show the position of the robot leg θ , position of the pivot point x that defines the stiffness of the PVSA, and the frequency of oscillations. The PVSA maximized the amplitude of oscillations $\theta \in [-30, +30]$ deg within three cycles. The stiffness was incrementally increased from 1.9 to 29.3 Nm rad⁻¹ within the limited window of adjustment around the equilibrium position of the spring $\theta \in [-5, +5]$ deg, see Fig. 12(a-i,ii) (green area and green dashed lines). We also see that the incremental change in stiffness – as proposed in (6) – resulted in a 32% increase of frequency, from 0.65 Hz to 0.86 Hz.

Figures 12(b-i), 12(b-ii), and 12(b-iii) show the experimental results for the PEA. The PEA operated with minimal amplitude and maximal stiffness in each oscillation cycle, as

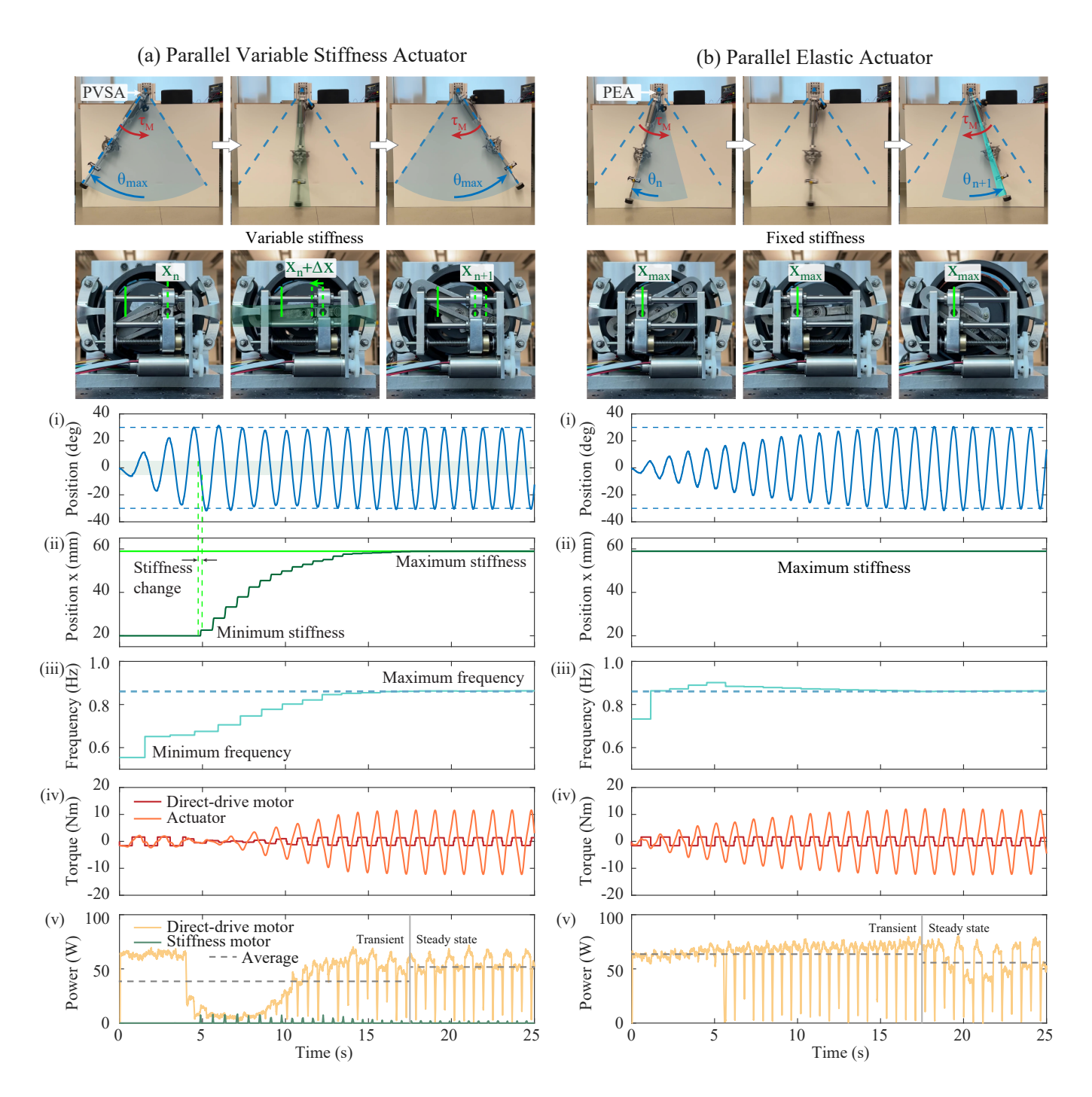


Fig. 12. Experiment. (a) The left column shows the results for the PVSA; the video of the experiment is provided in the supplementary material. (b) The right column shows the corresponding results for the PEA. The top rows show the oscillation of the leg. The second row shows the stiffness modulating mechanism, and the change of the pivot point during the experiment. In the PVSA, (a) the stiffness was changed from its minimum to its maximum value. In the PEA, (b) the stiffness was kept at its maximum value; the energy storage capacity of the actuator was the same during both experiments, (a) and (b). For each experiment, we show the (i) shaft angle, (ii) position of the pivot point, (iii) oscillation frequency, (iv) motor and actuator torque, (v) electrical power consumption of the direct-drive motor, and the motor used to modulate the spring stiffness.

opposed to the PVSA which operated with maximal amplitudes and minimal stiffness in each oscillation cycle. Also, without stiffness adaptation, the PEA required more cycles to achieve the maximal amplitude compared to the PVSA (12 cycles compared to 3 cycles), shown in Fig. 12(a-i). Finally, we note that, while the stiffness of the PEA was not varied, see 12(b-ii), the frequency of the leg was not constant, see

Fig. 12(b-iii). This effect is due to the amplitude-dependent frequency of nonlinear oscillators; oscillators with weakening force-deflection characteristics (Fig. 9) display decreasing frequency at increasing amplitudes, see Fig. 12(b-iii).

Figures 12(a-iv) and 12(b-iv) show the torque of the directdrive motor, and the actuator torque of the PVSA and the PEA, respectively. We observe that the actuator torque is progressively amplified – as predicted by (8) – from the maximal motor torque of 1.6 Nm (red lines) to the maximum actuator torque 11.6 Nm (orange lines). A comparable motor torque amplification would require a gearbox with a 7.25:1 gear ratio.

Figure 12(a-v) shows the power consumption of both the direct-drive motor (yellow line) and the motor used to change the stiffness of the PVSA (green line). During the transient period $(t \in [0, 17.5])$ s), the average power consumption of the PVSA was 39 W; the dip in the power plot is explained by the slight overshoot in Fig. 12(a-i) at $t \in [5, 10]$. During the transient period, the motor used to change the stiffness consumed an average 0.35 W power to incrementally increase stiffness from 1.9 to 29.3 Nm rad⁻¹ over 14 seconds, accounting for less than 1% of the total energy required to oscillate the robot leg. This result demonstrates the benefit of the PVSA to amplify force as required to oscillate a load by leveraging the proposed method to adapt the stiffness of the actuator at low energy cost. Figure 12(a-v) also shows that, during steady-state oscillations ($t \in [17.5, 25]$ s), the PVSA consumed an average power of 52 W. This power consumption is mainly due to the energy dissipated by the 3D-printed composite spring (Fig. 9).

Figure 12(b-v) shows the power consumption of the directdrive motor when the actuator was operated as a PEA. During the steady-state oscillations ($t \in [17.5, 25]$ s), the PEA consumed 56 W average power, which is approximately the same as the steady-state power of the PVSA. During the transient period ($t \in [0, 17.5]$ s), the PEA consumed 64 W average power, which was 64% higher than the transient power consumption of the PVSA. The difference between the transient power consumption of the PVSA and PEA can be attributed to the differences in the torque of the directdrive motor. There are two main reasons for the differences in torques of the PEA compared to the PVSA: (i) the increased internal energy dissipation due to the higher stiffness during the transient period of the PEA compared to the lower stiffness during the transient period of the PVSA (see Fig. 9), and (ii) the time delay in switching the motor torque (4). Although a time delay δt , mentioned in Section II-C (12), affects both the PVSA and the PEA, it affects the PEA more because the PEA operates with higher transient oscillation frequencies, see Fig. 12(a,b-iii), and the ability of the motor to do work decreases with higher oscillation frequencies.

Figure 12(a,b-v) shows that the PEA and PVSA have approximately the same steady-state power consumption while oscillating the leg with the same amplitude $(\pm 30^{\circ})$ and the same frequency (0.86 Hz). This result is consistent with the theoretical prediction illustrated in Fig. 4, where we show that the PEA and PVSA have the same efficiency when the PEA is operated at the resonant frequency. Figure 4 also shows that the efficiency of the PEA decreases if there is a mismatch between the oscillation frequency and the resonant frequency. To experimentally demonstrate the latter prediction, we repeated the experiment shown in Fig. 12(b) while offsetting the stiffness modulating motor from x = 60 mm (corresponding to the resonant frequency 0.86 Hz) to x = 55 mm (representing a 20% decreased non-resonant frequency), see Fig. 9.

Figure 13(a) shows the result of using the PEA with the non-

resonant stiffness (x=55 mm as opposed to x=60 mm). We observe that the PEA was able to achieve the desired resonant frequency (0.86 Hz) of the oscillatory motion, see Figure 13(a-iii), but was unable to achieve the desired amplitude ($\pm 30^{o}$) of the oscillatory motion, see Figure 13(a-i). This observation indicates a lower efficiency of the PEA when used at a non-resonant frequency compared to that of a PEA or PVSA used at the resonant frequency. This result supports our theoretical prediction shown in Fig. 4.

Finally, we tested whether the direct-drive motor alone could achieve the steady-state oscillatory motion shown in Figure 12(a,b-i) without the spring. To answer this question, we repeated the experiment while the spring was decoupled from the load. Figure 13(b) shows the experimental data. We observe that the motor was unable to oscillate the robot leg with the desired frequency (0.86 Hz) and the desired amplitude ($\pm 30^{\circ}$). This result demonstrates the benefit of using the 3D-printed composite spring.

V. DISCUSSION AND CONCLUSION

This paper presented a compact and modular design of a parallel variable stiffness actuator and showed the potential benefits of parallel variable stiffness actuation in amplifying the torque, energy, and power output of a relatively small motor in cyclic tasks. We detailed the design of a parallel variable stiffness actuator, which embodies a motor, a composite spring, and a mechanism to adjust the stiffness of the actuator. Finally, we experimentally verified the predicted benefits of the parallel variable stiffness actuator in an oscillatory task where a robotic leg was oscillated at limited amplitudes but increasing frequencies. The experiment showed that parallel variable stiffness actuation can provide significant force amplification together with an appreciable energetic benefit if the energy required to adapt the stiffness of the actuator is minimized.

In the remainder of this section, we discuss the limitations and future works to make PVSAs an energy efficient alternative to motors with gearboxes for oscillatory motion.

A. Composite Spring Design

One of the common limitations of compliant actuators, including PVSAs, is the low energy storage density of conventional steel springs [52]. Fiber reinforced 3D printing technology offers a convenient method to manufacture high energy-density composite springs such as the fiberglass spring used in this study. The added benefit of the 3D printing technology is to allow customization of spring geometries that are easier to integrate into a compact actuator.

While composite springs are lighter, easier, and cheaper to custom-make, they have a higher level of energy loss than traditional metal springs [53]. Creating energy efficient composite springs could enable the design of efficient high mass-energy density compliant actuators.

B. Energy regeneration

Instead of springs, electrical energy regeneration could be used to improve the efficiency of cyclic tasks [54]. Some

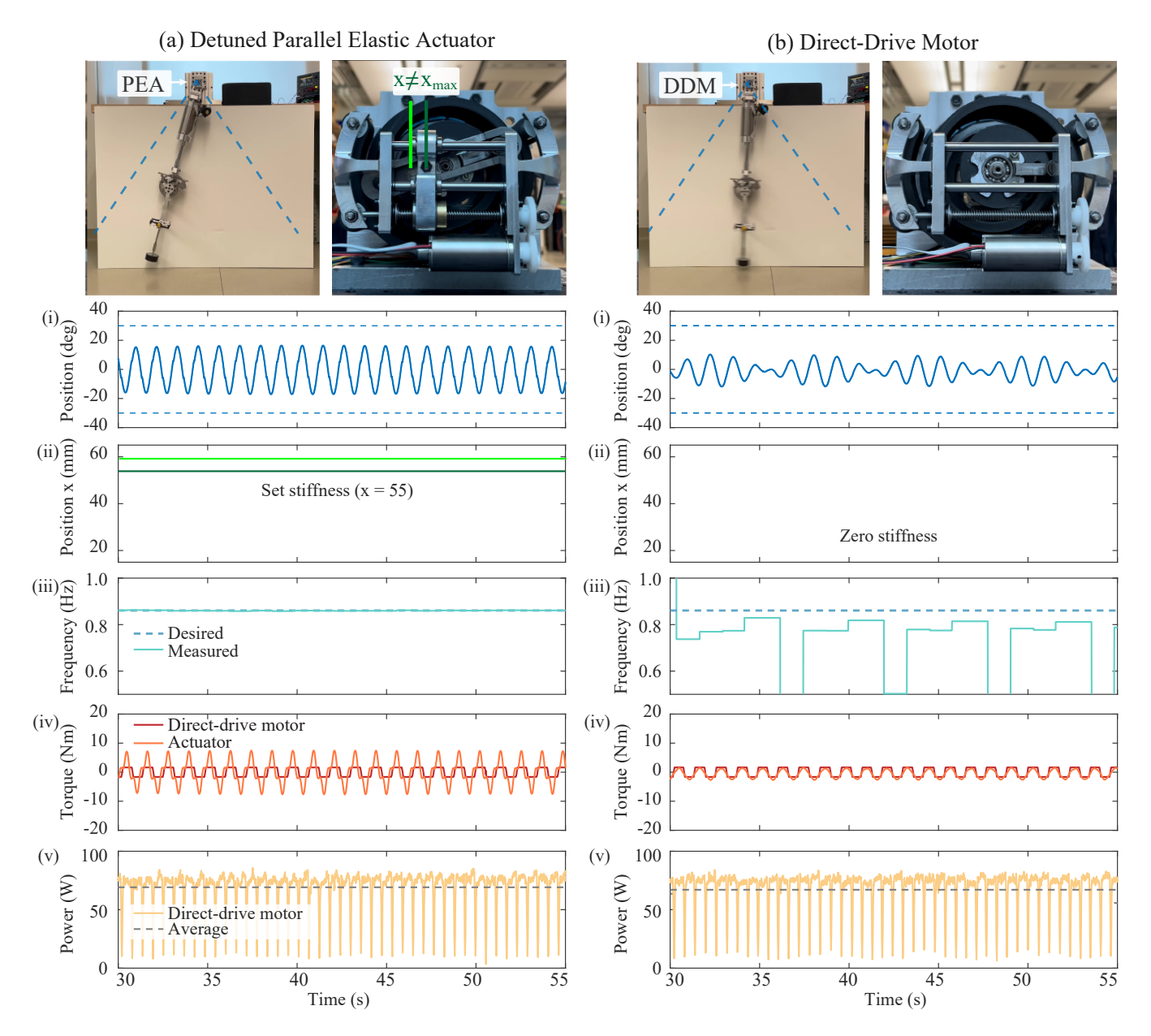


Fig. 13. Experiment with a detuned parallel elastic actuator and the direct-drive motor alone. (a) The PEA oscillates the leg at same frequency used in Fig. 12 (0.86 Hz) but uses a different stiffness (observe that here x = 55 mm instead of 60 mm in Fig. 12). (b) The direct-drive motor oscillates the leg with the spring disconnected. For each experiment, we show the (i) shaft angle, (ii) position of the pivot point, (iii) oscillation frequency, (iv) motor and actuator torque, (v) electrical power consumption of the drive motor. The plots are shown after 30 seconds of transient oscillation such that they can be compared to the steady-state data shown in Fig. 12.

motor-driven robotic joints have demonstrated an energy capture efficiency of 63% [55]. However, when accounting for both the energy capture efficiency and the efficiency of supplying the regenerated energy, the estimated overall efficiency may be no more than 40% [36].

Furthermore, motors cannot regenerate energy during static tasks, and they require energy to generate torque even if they do not do mechanical work. Consequently, when a task is energetically passive, springs can be more efficient at storing and returning energy than motors [56]. Springs have the ability to passively generate torque, which is especially useful for systems with significant static loading [57]. However, in oscillatory tasks, fixed-stiffness springs are the most efficient in

amplifying force and energy around their resonant frequency, which limits their practicality compared to motors, which are capable of energy regeneration at a wide range of frequencies. In order to efficiently store and return energy over a range of frequencies, an actuator with variable stiffness capability is required.

C. Series variable stiffness actuators

Similar to PVSAs, SVSAs can also be used to generate oscillatory motion over a range of frequencies. However, the ability of a SVSA to supply energy to the load during resonant oscillations depends on the reduction ratio of the gearbox placed between the motor and the spring. Without a large

gear reduction ratio, the motor must accelerate and decelerate rapidly to generate large inertial forces that compensate the spring force. As the motor moves rapidly, a large portion of the energy stored in the spring is transferred to the motor rather than the load. This limits the ability of SVSAs with low gear ratios to supply energy to the load compared to direct-driven PVSAs, see Section II-D (18).

One way to mitigate the mentioned issue is to use a gearbox with a large gear reduction ratio. However, a gearbox with a large gear reduction ratio adds mass and consequently lowers the power density of the actuator (aside from introducing a long transient to accumulate energy and increasing energy dissipation). One could also use a clutch to lock the motor, thereby helping to counter the spring force without using the motor [22], [58]. However, the motor must be unlocked to supply energy during the process of energy accumulation or to compensate for load-side energy dissipation, where a large gear reduction ratio is also needed. Therefore, SVSAs cannot simultaneously achieve a high energy transfer ratio between the spring and the load and high power density.

In Section II-D we have seen that PVSAs are not subject to the aforementioned limitation. However, PVSAs are limited in the motions they can generate compared to series spring actuators due to their fixed equilibrium position.

D. Parallel variable stiffness actuators

Design modifications are required to expand the energetic benefits of PVSAs to tasks that require modulation of the spring equilibrium position. For example, it may be beneficial to add a clutch that engages and disengages the spring mechanism [32] in order to control the timing of energy storage and release. This would allow the PVSA to effectively switch between a parallel variable stiffness spring (appropriate for elastic potential energy storage and return) and a DDM (appropriate for force and position control). In cyclic tasks with holding periods – pick-and-place tasks – the energy costs could be reduced by locking the spring, since it is not efficient to use the motor to compensate the spring force during the holding periods [59], [60].

A combination of both a spring-disengage clutch and a spring-lock clutch [61] would allow fully controllable energy storage and equilibrium control of the PVSA. Such PVSA could be used in mobile robots, where the robot may switch between tasks such as walking and lifting, which require different spring equilibrium positions and different timings to lock and release the energy stored by the spring. With these modifications, we aim to build PVSAs which can replace gearboxes in oscillatory tasks, without compromising power density and energy efficiency.

VI. APPENDIX

A. Energy transfer in parallel and series spring actuators

For parallel spring actuators, we have the following energy conservation law for unforced constant amplitude and constant frequency oscillations,

$$E = \frac{1}{2}kq_{\text{max}} = \frac{1}{2}(m_L + m_D)\dot{q}_{\text{max}}^2.$$

Consequently, the energy ratio of a parallel spring actuator is:

$$\frac{E_L}{E_S}\Big|_P = \frac{\frac{1}{2}m_L \dot{q}_{\max}^2}{\frac{1}{2}kq_{\max}^2} = \frac{m_L}{m_L + m_D} = \frac{1}{1 + \frac{m_D}{m_L}}.$$

For series spring actuators, where the actuator has an n_G : 1 gearbox between the motor and the spring, we have the following linear momentum and energy conservation laws for unforced constant amplitude and constant frequency oscillations,

$$m_L \dot{q}_{L \max} + n_G m_D \dot{q}_{D \max} = 0,$$

$$E = \frac{1}{2} k \Delta l_{\max}^2 = \frac{1}{2} m_L \dot{q}_{L \max}^2 + \frac{1}{2} n_G^2 m_D \dot{q}_{D \max}^2,$$
(25)

where Δl_{max} is the maximal deflection of the spring. Using (25), we find the energy ratio of series spring actuators:

$$\frac{E_L}{E_S}\Big|_S = \frac{\frac{1}{2}m_L\dot{q}_{L\,\text{max}}^2}{\frac{1}{2}k\Delta l_{\text{max}}^2} = \frac{n_G^2m_D}{m_L + n_G^2m_D} = \frac{n_G^2\frac{m_D}{m_L}}{1 + n_G^2\frac{m_D}{m_U}}.$$

B. Energy cost of stiffness modulation

To estimate the energy cost of changing the stiffness of the actuator k(x) (24), we assume that the mechanism that changes the stiffness is non-backdrivable such that holding the motor position x requires no energy (this is ensured by the lead screw in our design, see Fig. 8). Also, we assume a high transmission ratio (provided by the lead screw), such that Joule losses are negligible compared to the cost of rapidly accelerating and decelerating the motor that changes the spring stiffness. Finally, we assume that there is no energy regeneration, and that the motor must supply energy to do both positive and negative work.

Given the aforementioned assumptions, we estimate the energy cost of changing stiffness ΔE_{kx} , by multiplying (2) with \dot{x} , taking the absolute value of the resulting expression (because we assume that the motor has to supply energy to do both positive and negative work), and then integrating the result from t to $t + \Delta t$,

$$\underbrace{\int_{t}^{t+\Delta t} |F_{S}\dot{x}| dt}_{\Delta E_{kx}} \leq \underbrace{\int_{t}^{t+\Delta t} \frac{1}{2} \left| \frac{dk}{dx} \dot{x} \right| q^{2} dt}_{\Delta E_{k}} + \underbrace{\int_{t}^{t+\Delta t} m_{S} |\ddot{x}\dot{x}| dt}_{\Delta E_{x}}, \quad (26)$$

where Δt is the short time for the oscillator to move from q(t) = 0 to $q(t + \Delta t) = \Delta q \ll q_{\text{max}}$ at each half-cycle.

The upper bound for ΔE_k is defined by (20). In order to compute the upper bound for ΔE_x we assume that the motor is speed limited $|\dot{x}| \leq \dot{x}_{\rm max}$ and has a critically damped dynamics, characterized by the time constant τ_x used in (12), such that the maximal acceleration of the motor is,

$$\ddot{x}_{\text{max}} = 2\frac{\dot{x}_{\text{max}}}{\tau_x}.$$
 (27)

Using the second integral on the right-hand side of (26), and assuming that the motor moves with maximal constant acceleration (27) from t to $t + \Delta t$, we find

$$\Delta E_x \le \frac{1}{2} m_S \ddot{x}_{\text{max}}^2 \Delta t^2. \tag{28}$$

We aim to compare ΔE_x with the energy supplied by the direct-drive motor during each half-cycle of the oscillatory motion (5),

$$|\Delta E_n| = \frac{1}{2} |\Delta k| q_{\text{max}}^2. \tag{29}$$

In order to compute the change of the spring stiffness Δk in (29), we assume k = k(x) as used in (24), and consider the constant acceleration (27) used in (28), to obtain:

$$|\Delta k| = \left| \frac{dk(x)}{dx} \right|_{x_{q=0}} \Delta x \right| \le \frac{1}{2} \left| \frac{dk(x)}{dx} \right|_{x_{q=0}} |\ddot{x}_{\text{max}} \Delta t^2.$$
 (30)

Based on (28)–(30), the ratio between the energy required to accelerate (decelerate) the motor ΔE_x , and the energy supplied by the direct-drive motor during each half-cycle of the oscillatory motion is:

$$\frac{\Delta E_x}{|\Delta E_n|} \le \frac{2m_S \dot{x}_{\text{max}}}{\tau_x \frac{dk(x)}{dx} \Big|_{x_{t=0}} q_{\text{max}}^2}.$$
 (31)

Relation (31) shows that reducing the motor mass and the inertia of the stiffness modulating mechanism (smaller m_S) could reduce the energy cost of acceleration and deceleration, while increasing the speed (larger $\dot{x}_{\rm max}$) and reducing the time constant (smaller τ_x) would increase the energy cost of stiffness modulation. In general, (31) can be used to guide the design of the stiffness modulating mechanism in order to keep the energy cost of changing the stiffness of the actuator low compared to the energy supplied by the direct-drive motor.

REFERENCES

- J. Zhang, J. Sheng, C. T. O'Neill, C. J. Walsh, R. J. Wood, J.-H. Ryu, J. P. Desai, and M. C. Yip, "Robotic artificial muscles: Current progress and future perspectives," *IEEE Transactions on Robotics*, vol. 35, no. 3, pp. 761–781, 2019.
- [2] D. J. Braun and M. Goldfarb, "A control approach for actuated dynamic walking in biped robots," *IEEE Transactions on Robotics*, vol. 25, no. 6, pp. 1292–1303, 2009.
- [3] P. M. Wensing, A. Wang, S. Seok, D. Otten, J. Lang, and S. Kim, "Proprioceptive actuator design in the MIT cheetah: Impact mitigation and high-bandwidth physical interaction for dynamic legged robots," *IEEE Transactions on Robotics*, vol. 33, no. 3, pp. 509–522, 2017.
- [4] D. V. Gealy, S. McKinley, B. Yi, P. Wu, P. R. Downey, G. Balke, A. Zhao, M. Guo, R. Thomasson, A. Sinclair, P. Cuellar, Z. McCarthy, and P. Abbeel, "Quasi-direct drive for low-cost compliant robotic manipulation," in *IEEE International Conference on Robotics and Automation*, (Montreal, Canada), pp. 437–443, May 2019.
- [5] S. Yu, T.-H. Huang, X. Yang, C. Jiao, J. Yang, Y. Chen, J. Yi, and H. Su, "Quasi-direct drive actuation for a lightweight hip exoskeleton with high backdrivability and high bandwidth," *IEEE/ASME Transactions on Mechatronics*, vol. 25, no. 4, pp. 1794–1802, 2020.
- [6] H. Zhu, C. Nesler, N. Divekar, V. Peddinti, and R. Gregg, "Design principles for compact, backdrivable actuation in partial-assist powered knee orthoses," *IEEE/ASME Transactions on Mechatronics*, vol. 4435, no. c. 2021.
- [7] D. J. Braun, M. Howard, and S. Vijayakumar, "Exploiting variable stiffness in explosive movement tasks," in *Proceedings of Robotics: Science and Systems*, (Los Angeles, CA, USA), June-July 2011.
- [8] D. J. Braun, M. Howard, and S. Vijayakumar, "Optimal variable stiffness control: Formulation and application to explosive movement tasks," *Autonomous Robots*, vol. 33, no. 3, pp. 237–253, 2012.
- [9] D. J. Braun, F. Petit, F. Huber, S. Haddadin, P. van der Smagt, A. Albu-Schäffer, and S. Vijayakumar, "Robots driven by compliant actuators: Optimal control under actuation constraints," *IEEE Transactions on Robotics*, vol. 29, no. 5, pp. 1085–1101, 2013.
- [10] S. H. Collins, M. Bruce Wiggin, and G. S. Sawicki, "Reducing the energy cost of human walking using an unpowered exoskeleton," *Nature*, vol. 522, no. 7555, pp. 212–215, 2015.

- [11] R. Nasiri, A. Ahmadi, and M. N. Ahmadabadi, "Reducing the energy cost of human running using an unpowered exoskeleton," *IEEE Transac*tions on Neural Systems and Rehabilitation Engineering, vol. 26, no. 10, pp. 2026–2032, 2018.
- [12] C. S. Simpson, C. G. Welker, S. D. Uhlrich, S. M. Sketch, R. W. Jackson, S. L. Delp, S. H. Collins, J. C. Selinger, and E. W. Hawkes, "Connecting the legs with a spring improves human running economy," *Journal of Experimental Biology*, vol. 222, no. 17, 2019.
- [13] A. Sutrisno and D. J. Braun, "Enhancing mobility with quasi-passive variable stiffness exoskeletons," *IEEE Transactions on Neural Systems* and Rehabilitation Engineering, vol. 27, no. 3, pp. 487–496, 2019.
- [14] A. Sutrisno and D. J. Braun, "How to run 50% faster without external energy," *Science Advances*, vol. 6, no. 13, pp. 1–11, 2020.
- [15] T. Zhou, C. Xiong, J. Zhang, D. Hu, W. Chen, and X. Huang, "Reducing the metabolic energy of walking and running using an unpowered hip exoskeleton," *Journal of NeuroEngineering and Rehabilitation*, vol. 18, no. 1, pp. 1–15, 2021.
- [16] G. Pratt and M. Williamson, "Series elastic actuators," in *IEEE/RSJ International Conference on Intelligent Robots and Systems*, vol. 1, (Pittsburgh, PA, USA), pp. 399–406, August 1995.
- [17] J. W. Hurst, J. E. Chestnutt, and A. A. Rizzi, "An actuator with physically variable stiffness for highly dynamic legged locomotion," in *IEEE International Conference on Robotics and Automation*, vol. 5, (New Orleans, LA, USA), pp. 4662–4667 Vol.5, April-May 2004.
- [18] J. Sun, Z. Guo, Y. Zhang, X. Xiao, and J. Tan, "A novel design of serial variable stiffness actuator based on an archimedean spiral relocation mechanism," *IEEE/ASME Transactions on Mechatronics*, vol. 23, no. 5, pp. 2121–2131, 2018.
- [19] J. Sun, Z. Guo, D. Sun, S. He, and X. Xiao, "Design, modeling and control of a novel compact, energy-efficient, and rotational serial variable stiffness actuator (SVSA-II)," *Mechanism and Machine Theory*, vol. 130, pp. 123–136, 2018.
- [20] D. Ragonesi, S. Agrawal, W. Sample, and T. Rahman, "Series elastic actuator control of a powered exoskeleton," in *International Conference* of the IEEE Engineering in Medicine and Biology Society, (Boston, MA, USA), pp. 3515–3518, August - September 2011.
- [21] E. J. Rouse, L. M. Mooney, E. C. Martinez-Villalpando, and H. M. Herr, "Clutchable series-elastic actuator: Design of a robotic knee prosthesis for minimum energy consumption," in *IEEE International Conference* on Rehabilitation Robotics, (Seattle, WA, USA), pp. 1–6, June 2013.
- [22] B. Convens, D. Dong, R. Furnemont, T. Verstraten, P. Cherelle, D. Lefeber, and B. Vanderborght, "Modeling, design and test-bench validation of a semi-active propulsive ankle prosthesis with a clutched series elastic actuator," *IEEE Robotics and Automation Letters*, vol. 4, no. 2, pp. 1823–1830, 2019.
- [23] A. F. Azocar, L. M. Mooney, J. F. Duval, A. M. Simon, L. J. Hargrove, and E. J. Rouse, "Design and clinical implementation of an open-source bionic leg," *Nature Biomedical Engineering*, vol. 4, no. 10, pp. 941–953, 2020.
- [24] J. Geeroms, L. Flynn, R. Jimenez-Fabian, B. Vanderborght, and D. Lefeber, "Ankle-knee prosthesis with powered ankle and energy transfer for CYBERLEGs α-prototype," in *International Conference on Rehabilitation Robotics*, (Seattle, WA, USA), pp. 1–6, June 2013.
- [25] B. Ugurlu, C. Doppmann, M. Hamaya, P. Forni, T. Teramae, T. Noda, and J. Morimoto, "Variable ankle stiffness improves balance control: Experiments on a bipedal exoskeleton," *IEEE/ASME Transactions on Mechatronics*, vol. 21, no. 1, pp. 79–87, 2016.
- [26] S. Wolf, O. Eiberger, and G. Hirzinger, "The DLR FSJ: Energy based design of a variable stiffness joint," in *IEEE International Conference* on Robotics and Automation, (Shanghai, China), pp. 5082–5089, May 2011.
- [27] S. Wang, W. van Dijk, and H. van der Kooij, "Spring uses in exoskeleton actuation design," in *IEEE International Conference on Rehabilitation Robotics*, (Zurich, Switzerland), pp. 1–6, June-July 2011.
- [28] W. Roozing, Z. Ren, and N. G. Tsagarakis, "An efficient leg with series-parallel and biarticular compliant actuation: design optimization, modeling, and control of the eleg," *The International Journal of Robotics Research*, vol. 40, no. 1, pp. 37–54, 2021.
- [29] W. D. van Dorsser, R. Barents, B. M. Wisse, M. Schenk, and J. L. Herder, "Energy-free adjustment of gravity equilibrators by adjusting the spring stiffness," *Proceedings of the Institution of Mechanical Engineers, Part C: Journal of Mechanical Engineering Science*, vol. 222, no. 9, pp. 1839–1846, 2008.
- [30] J. Kim, J. Moon, J. Ryu, and G. Lee, "CVGC-II: A new version of a compact variable gravity compensator with a wider range of variable torque and energy-free variable mechanism," *IEEE/ASME Transactions* on Mechatronics, vol. 27, no. 2, pp. 678–689, 2022.

- [31] U. Mettin, P. X. La Hera, L. B. Freidovich, and A. S. Shiriaev, "Parallel elastic actuators as a control tool for preplanned trajectories of underactuated mechanical systems," *The International Journal of Robotics Research*, vol. 29, no. 9, pp. 1186–1198, 2010.
- [32] D. F. B. Haeufle, M. D. Taylor, S. Schmitt, and H. Geyer, "A clutched parallel elastic actuator concept: Towards energy efficient powered legs in prosthetics and robotics," in *IEEE RAS EMBS International Conference on Biomedical Robotics and Biomechatronics*, (Rome, Italy), pp. 1614–1619, June 2012.
- [33] M. Grimmer, M. Eslamy, S. Gliech, and A. Seyfarth, "A comparison of parallel- and series elastic elements in an actuator for mimicking human ankle joint in walking and running," in *IEEE International Conference* on Robotics and Automation, (Saint Paul, MN, USA), pp. 2463–2470, May 2012.
- [34] M. Plooij and M. Wisse, "A novel spring mechanism to reduce energy consumption of robotic arms," in 2012 IEEE/RSJ International Conference on Intelligent Robots and Systems, (Vilamoura-Algarve, Portugal), pp. 2901–2908, October 2012.
- [35] B. Na and K. Kong, "Control power reduction and frequency bandwidth enlargement of robotic legs by nonlinear resonance," *IEEE/ASME Transactions on Mechatronics*, vol. 20, no. 5, pp. 2340–2349, 2015.
- [36] M. Plooij, M. Wisse, and H. Vallery, "Reducing the energy consumption of robots using the bidirectional clutched parallel elastic actuator," *IEEE Transactions on Robotics*, vol. 32, no. 6, pp. 1512–1523, 2016.
- [37] Y. Li, X. Guan, Z. Li, Z. Tang, B. Penzlin, Z. Yang, S. Leonhardt, and L. Ji, "Analysis, design, and preliminary evaluation of a parallel elastic actuator for power-efficient walking assistance," *IEEE Access*, vol. 8, pp. 88060–88075, 2020.
- [38] J. V. Nicholson, S. Gart, J. Pusey, and J. E. Clark, "Evaluating the efficacy of parallel elastic actuators on high-speed, variable stiffness running," in *IEEE/RSJ International Conference on Intelligent Robots* and Systems, (Las Vegas, NV, USA), pp. 3641–3648, Oct-Jan 2021.
- [39] X. Liu, A. Rossi, and I. Poulakakis, "A switchable parallel elastic actuator and its application to leg design for running robots," *IEEE/ASME Transactions on Mechatronics*, vol. 23, no. 6, pp. 2681–2692, 2018.
- [40] C. W. Mathews and D. J. Braun, "Parallel variable stiffness actuators," in IEEE/RSJ International Conference on Intelligent Robots and Systems, (Prague, Czech Republic), pp. 8225–8231, September 2021.
- [41] V. Chalvet and D. J. Braun, "Criterion for the design of low-power variable stiffness mechanisms," *IEEE Transactions on Robotics*, vol. 33, no. 4, pp. 1002–1010, 2017.
- [42] D. J. Braun, V. Chalvet, T.-H. Chong, S. S. Apte, and N. Hogan, "Variable stiffness spring actuators for low-energy-cost human augmentation," *IEEE Transactions on Robotics*, vol. 35, no. 6, pp. 1435–1449, 2019.
- [43] T. Verstraten, P. Beckerle, R. Furnémont, G. Mathijssen, B. Vanderborght, and D. Lefeber, "Series and parallel elastic actuation: Impact of natural dynamics on power and energy consumption," *Mechanism and Machine Theory*, vol. 102, pp. 232–246, 2016.
- [44] A. Calanca and T. Verstraten, "An energy efficiency index for elastic actuators during resonant motion," *Robotica*, vol. 40, no. 5, p. 1450–1474, 2022.
- [45] S. M. Kabir, K. Mathur, and A. F. M. Seyam, "A critical review on 3D printed continuous fiber-reinforced composites: History, mechanism, materials and properties," *Composite Structures*, vol. 232, p. 111476, 2020
- [46] Z. Hou, X. Tian, Z. Zheng, J. Zhang, L. Zhe, D. Li, A. V. Malakhov, and A. N. Polilov, "A constitutive model for 3D printed continuous fiber reinforced composite structures with variable fiber content," *Composites Part B: Engineering*, vol. 189, no. October 2019, p. 107893, 2020.
- [47] J. M. Muñoz-Guijosa, D. Fernández Caballero, V. Rodríguez De La Cruz, J. L. Muñoz Sanz, and J. Echávarri, "Generalized spiral torsion spring model," *Mechanism and Machine Theory*, vol. 51, pp. 110–130, 2012.
- [48] Y. Li, Z. Li, B. Penzlin, Z. Tang, Y. Liu, X. Guan, L. Ji, and S. Leonhardt, "Design of the clutched variable parallel elastic actuator (CVPEA) for lower limb exoskeletons," in *International Conference* of the IEEE Engineering in Medicine and Biology Society, (Berlin, Germany), pp. 4436–4439, July 2019.
- [49] A. Jafari, N. G. Tsagarakis, I. Sardellitti, and D. G. Caldwell, "A new actuator with adjustable stiffness based on a variable ratio lever mechanism," *IEEE/ASME Transactions on Mechatronics*, vol. 19, no. 1, pp. 55–63, 2014.
- [50] K. W. Hollander and T. G. Sugar, "Design of lightweight lead screw actuators for wearable robotic applications," *Journal of Mechanical Design*, vol. 128, pp. 644–648, 07 2005.

- [51] T. Zhang and D. J. Braun, "Human driven compliant transmission mechanism," in *IEEE International Conference on Robotics and Automation*, (Xi'an, China), pp. 7094–7099, May-June 2021.
- [52] J. D. Madden, "Mobile robots: Motor challenges and materials solutions," *Science*, vol. 318, no. 5853, pp. 1094–1097, 2007.
- [53] M. F. Ashby, Materials selection in mechanical design. Pergamon Press, 2 ed., 1999.
- [54] B. Laschowski, R. S. Razavian, and J. McPhee, "Simulation of stand-to-sit biomechanics for robotic exoskeletons and prostheses with energy regeneration," *IEEE Transactions on Medical Robotics and Bionics*, vol. 3, no. 2, pp. 455–462, 2021.
- [55] S. Seok, A. Wang, M. Y. Chuah, D. Otten, J. Lang, and S. Kim, "Design principles for highly efficient quadrupeds and implementation on the MIT Cheetah robot," in *IEEE International Conference on Robotics and Automation*, (Karlsruhe, Germany), pp. 3307–3312, May 2013.
- [56] S. Rezazadeh, A. Abate, R. L. Hatton, and J. W. Hurst, "Robot leg design: A constructive framework," *IEEE Access*, vol. 6, pp. 54369– 54387, 2018.
- [57] A. Mazumdar, S. J. Spencer, C. Hobart, J. Salton, M. Quigley, T. Wu, S. Bertrand, J. Pratt, and S. P. Buerger, "Parallel elastic elements improve energy efficiency on the STEPPR bipedal walking robot," *IEEE/ASME Transactions on Mechatronics*, vol. 22, no. 2, pp. 898–908, 2017.
- [58] E. J. Rouse, L. M. Mooney, and H. M. Herr, "Clutchable series-elastic actuator: Implications for prosthetic knee design," *The International Journal of Robotics Research*, vol. 33, no. 13, pp. 1611–1625, 2014.
- [59] H. Goya, K. Matsusaka, M. Uemura, Y. Nishioka, and S. Kawamura, "Realization of high-energy efficient pick-and-place tasks of SCARA robots by resonance," in *IEEE/RSJ International Conference on Intelligent Robots and Systems*, (Vilamoura-Algarve, Portugal), pp. 2730– 2735, October 2012.
- [60] S. Y. Kim and D. J. Braun, "Novel variable stiffness spring mechanism: Modulating stiffness independent of the energy stored by the spring," in *IEEE International Conference on Intelligent Robots and Systems*, (Prague, Czech Republic), pp. 8232–8237, September 2021.
- [61] M. Plooij, W. Wolfslag, and M. Wisse, "Clutched elastic actuators," IEEE/ASME Transactions on Mechatronics, vol. 22, no. 2, pp. 739–750, 2017.



Chase W. Mathews received the B.S degree in Mechanical Engineering from Auburn University, USA, in 2019. He is currently a Ph.D. student at the Advanced Robotics and Control Laboratory within the Center for Rehabilitation Engineering and Assistive Technology at Vanderbilt University. His research interests include wearable robotics and human augmentation devices.



David J. Braun (M'09) received the Ph.D. degree in mechanical engineering from Vanderbilt University, Nashville, TN, USA, in 2009. He is Assistant Professor of Mechanical Engineering and Computer Engineering at Vanderbilt University, where he leads the Advanced Robotics and Control Laboratory. Prior to joining Vanderbilt, he was visiting researcher with the Institute for Robotics and Mechatronics at the German Aerospace Center, postdoctoral research fellow with the Statistical Machine Learning and Motor Control Group at the University of Edinburgh,

and Founding Faculty of Singapore University of Technology and Design.

Dr. Braun's research interests include dynamical systems, optimal control, and robotics. He received the IEEE King-Sun Fu Transactions on Robotics Memorial Best Paper Award in 2014, and the National Science Foundation CAREER Award in 2022. He was Scientific Program Co-Chair of the 2015 IEEE International Conference on Rehabilitation Robotics, Area Chair of the 2018 Robotics: Science and Systems Conference, and Associate Editor of the 2019-2020 IEEE International Conference on Robotics and Automation.